AMERICAN UNIVERSITY OF BEIRUT

MATHEMATICAL MODELING AND PARAMETER ESTIMATION OF BASAL-GANGLIA PROJECTING NEURONS IN THE ZEBRA FINCH

by
AHMAD MOHAMMAD SIBAHI

A thesis
submitted in partial fulfillment of the requirements
for the degree of Master of Science in Biomedical Engineering
to the Department of Biomedical Engineering
of Maroun Semaan Faculty of Engineering and Architecture
at the American University of Beirut

Beirut, Lebanon
September 2020

AMERICAN UNIVERSITY OF BEIRUT

MATHEMATICAL MODELING AND PARAMETER ESTIMATION OF BASAL-GANGLIA PROJECTING NEURONS IN THE ZEBRA FINCH

by

AHMAD MOHAMMAD SIBAHI

Approved by:

Arij Daou	
[Dr. Arij Daou, Assistant Professor] [Biomedical Engineering]	Advisor
Firas Kobeissy	
[Dr. Firas Kobeissy, Assistant Professor] [Biochemistry and Molecular Biology]	Co-Advisor
Jason Amatoury	
[Dr. Jason Amatoury, Assistant Professor] [Biomedical Engineering]	Member of Committee
Ghanem Oweis	
[Dr. Ghanem Oweis, Associate Professor] [Mechanical Engineering]	Member of Committee

Date of thesis/dissertation defense: [September 4, 2020]

AMERICAN UNIVERSITY OF BEIRUT

THESIS, DISSERTATION, PROJECT RELEASE FORM

Student Name: _____Sibahi_____Ahmad_____Mohammad_
Last First Middle

● Master's Thesis ○ Master's Project ○ Doctoral Dissertation

[X] I authorize the American University of Beirut to: (a) reproduce hard or electronic copies of my thesis, dissertation, or project; (b) include such copies in the archives and digital repositories of the University; and (c) make freely available such copies to third parties for research or educational purposes.

[ ] I authorize the American University of Beirut, to: (a) reproduce hard or electronic copies of it; (b) include such copies in the archives and digital repositories of the University; and (c) make freely available such copies to third parties for research or educational purposes
after : **One ---- year from the date of submission of my thesis, dissertation, or project.**

Two ---- years from the date of submission of my thesis, dissertation, or project.

Three ---- years from the date of submission of my thesis, dissertation, or project.

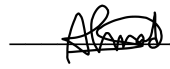

_____08-09-2020_____

Signature Date

This form is signed when submitting the thesis, dissertation, or project to the University Libraries

CONTENTS

ACKNOWLEDGMENTS…….. 1

.

ABSTRACT……... 2

LIST OF ILLUSTRATIONS…… 3

LIST OF TABLES…….. 4

Chapter

I. INTRODUCTION……..……. 5

II. LITERATURE REVIEW…..…… 10

A. Electrophysiological properties of HVC neurons...……. 10

B. Intrinsic plasticity of HVC neurons ...……. 14

C. Mathematical modeling of HVCx pyramidal neurons & its challenges... 17

III. MATERIAL AND METHODS.…...……. 21

A. Brain Slice Electrophysiology ...……. 21

B. Single Compartment Modeling …...……..... 21

IV. RESULTS AND DISCUSSION..…...…….. 27

V. CONCLUSION 42

Appendix

REFERENCES..... 44

ACKNOWLEDGMENTS

First and foremost, I would like to thank God Almighty for giving me the strength, knowledge, ability, and opportunity to undertake this research study and to persevere and complete it satisfactorily. Without his blessings, this achievement would not have been possible.

I would like also to thank my supervisor Dr. Arij Daou for his dedicated support and guidance. Dr. Arij continuously provided encouragement and was always willing and enthusiastic to assist in any way he could throughout the research project.

My sincere thanks go to an awesome family whom I have been always passionate and proud to be part of, “Insight Club Family”, for showing enough care and showering me with beautiful du’as in my journey at AUB.

Finally, from the bottom of my heart I would like to say big thank you to my parents, grandmother, and siblings whose love and guidance are with me in whatever I pursue. I am also thankful to my colleagues and my best friend Youssef Al Falah for providing me with unwavering support and endless reassurance throughout the process of researching and writing this thesis. May Allah bless you all with good health, wealth and prosperity in your life and reward you a home for you in Jannah! Ameen.

AN ABSTRACT OF THE THESIS OF

Ahmad Mohammad Sibahi for Master of Science
Major: Biomedical Engineering

Title: Mathematical modeling and parameter estimation of basal ganglia projecting neurons in the zebra finch

While the nonlinearity and complexity of biological phenomena keeps much of the intricate details of science mysterious, computational modeling can help unveil the dynamics and functionalities of such complex phenomena. The nucleus HVC (proper name) within the avian analog of mammal premotor cortex produces stereotyped instructions through the motor pathway leading to precise, learned vocalization by songbirds. The basal ganglia projecting HVC neurons (known as HVC_X) are a major class of neurons that project to Area X (avian basal ganglia) and play an essential role in the orchestration of the neural circuitry that guides the bird's learning and production mechanisms of his song. Huge efforts are being put onto developing realistic neural networks of HVC neurons and their associated networks, yet all of these modeling efforts are falling short due to the lack of appropriate models describing the intrinsic properties of HVC_X neurons themselves. In this research, we developed a single compartment conductance-based model to replicate the neurophysiological firing patterns and properties seen the HVC_X neurons of the zebra finch. The conductance-based model for HVC neurons was developed based on current-clamp data collected at the University of Chicago. Simulations of these model neurons were performed using MATLAB and XPPAUT. The modeled neurons are able to capture the spikes' timing as well as the details of the spikes' morphology and heuristics such as: spike amplitude, threshold, spike width, depolarization and repolarization segments. The careful fitting conducted unveiled important details about the intrinsic properties that these neurons exhibit in singing birds and built up on recent results that related ionic currents' magnitudes to features of song. The result is an improved characterization of the HVC_X neurons responsible for song production in the songbird and will be used in future studies to unveil the intricate circuitry that governs the overall process of bird's song.

ILLUSTRATIONS

Figure		Page
1.	Schematic of the song system.....	8
2.	Biological recordings of HVC neurons…….....	11
3.	Individual birds have uniform and distinct HVC_X intrinsic properties: spike waveforms…….....	15
4.	A scatter plot of all 151 manually modeled neurons showing the two conductances that varied the most across the population, g_{Na} and g_{SK}..	16
5.	Model simulations for HVC neurons…….....	18
6.	Heterogeneity across the various biological recordings.…….....	27
7.	Tuning of Na^+ and K^+ parameters to match the biological spikes…….	30
8.	Brute force search results...…….....	32
9.	Tuning of Na^+ and K^+ parameters to match the biological spikes for Neuron 3 of Red 240 bird...…….....	35
10.	Simulations and parameters estimations of the model parameters.....	37
11.	Steady-state activation functions for the fast gating variables that controls the activation/inactivation kinetics of the Na^+ and K^+ currents.	38
12.	Uniformity between modeled neurons from the same bird and different clustering across each other…….…….....	40

TABLES

Table		Page
1.	Ranges for the 11 different Na^+ and K^+ related parameters that played a crucial role in the fitting of our 30 different neurons.....	33

CHAPTER I

INTRODUCTION

Circuits of neurons in the brain are very complicated: because of the multiple nonlinearities, different types of neurons, complex dendritic geometries, diverse connectivity patterns and dependencies on learning and development, the cortex and other neuronal circuits constitute the most complex systems ever studied by science. Perhaps not surprisingly, the computational power that emerges from such circuits is astounding; neuronal networks are responsible for diverse cognitive phenomena such as seeing, smelling, remembering, planning and so on. Computational neuroscience is a field that is focused on understanding and describing biologically plausible phenomena related to neurons and their underlying networks, their physiology and their dynamics. The neuron itself is a very complex system composed of thousands if not millions of subparts that work in synchrony to orchestrate its behavior (spiking). Moreover, neurons regulate their intrinsic physiological properties but how these properties contribute to network dynamics and its plasticity remains unclear. One reason contributing to the lack of this clarity is because we don't have a clear understanding of how the various parts of the neuron work together to generate its behavior, something that computational modeling can help unveil.

One of the keystone questions in biology in general and neuroscience in specific is how simple or complex your model has to be to understand a given biological phenomena? That certainly depends on the questions being asked and the system under investigation, but what is really considered a "good model" and how detailistic your model needs to get given that biological models are highly nonlinear

and extremely complex? Nonlinear models of biological phenomena had been extensively used and studied by physicists and mathematicians and the applications of nonlinear methods are employed in several evolutionary, ecologic, physiologic, biochemical and neurological processes. Nonlinear analysis was successful in modeling not only basic cellular and molecular data but also complex cognitive processes and behavioral interactions (Mattei 2014). Given the nonlinearity of the various brain mechanisms, is it sufficient to build up with a model that replicates (or gets tangent to replicating) a neural trace? A good model should not only be based on pure biological assumptions and replicate the experimental results but also generate predictions about the behavior of the biological system under different stimuli, which could then be tested and verified experimentally to check the validity of the model. Nowadays, although neuroscience is becoming more of a quantitative science, but still at the level of small biological molecules there are many unsolved issues, involving stochasticity and nonlinearity, which need more investigation on both levels theoretically and experimentally (Donze et al. 2010). But the main challenge in modeling of neuronal systems is the estimation of the model parameters and understanding its nonlinear states. This is considered a major issue in all of biological systems because it is the corner stone in achieving quantitative and qualitative information from dynamical and structured models of these systems (Mansouri et al. 2014).

Detailed models have been successful in emulating neuronal firing patterns observed *in vitro* or *in vivo*. Primarily, computation of such detailed models has been possible due to significant technological advances that help solve differential equations in multiple dimensions. On one hand, detailed mathematical models are necessary to account for all the known components but on the other hand these detailed models

possess redundant parameters which often lead to an unnecessary increase in the cost of computation. With the hindsight, while it's impossible to know the functionalities of all the ingredients of a neuron to appropriately model it, the more we know about the internal house of the neuron the better the model. Even then, there are different established ways and techniques to model neurons, some that are biologically realistic and some are not, to study their functionalities at the intrinsic and network levels.

Birdsong learning is a well-established model for complex vocal learning. The acquisition and production of birdsong occurs through a set of brain nuclei that form a well-characterized network (Fig. 1). Cortical nucleus HVC plays a key role in the song system. Neurons in the HVC serve the role of the conductor of the song, having a pattern-generating role coding for syllable order and controlling the overall temporal structure of birdsong. The HVC contains three neural populations: neurons that project to the RA (robust nucleus of arcopallium) known as HVC_{RA}, neurons that project to Area X (of the avian basal ganglia) known as HVC_{X}, and HVC interneurons (HVC_{INT}). These three populations are interconnected with specific patterns of excitatory and inhibitory connectivity (Mooney and Prather 2005), and they fire with characteristic patterns both *in vivo* and *in vitro* (Mooney 2000, Long, Jin et al. 2010, Daou et al. 2013, Daou and Margoliash 2020). Precisely how neurons in HVC encode song sequence is poorly understood. Models of how neurons might be organized and interconnected have been proposed (Troyer and Doupe 2000, Drew and Abbott 2003, Abarbanel, Gibb et al. 2004, Abarbanel, Talathi et al. 2004, Mooney and Prather 2005, Li and Greenside 2006, Katahira, Okanoya et al. 2007, Gibb, Gentner et al. 2009, Gibb, Gentner et al. 2009, Jin 2009, Long, Jin et al. 2010) and techniques for calibrating HVC

models are being developed, but a complete biophysical model is limited by the lack of detailed understanding of the properties of the component neurons.

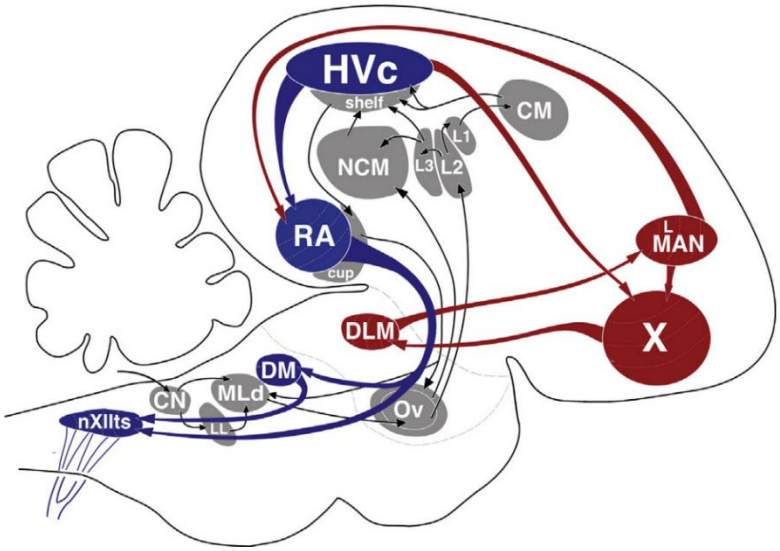

Figure 1: *Schematic of the song system (sagittal view). This figure shows that HVC HVC (used as a proper name, cortical analog in avians) includes interneurons (HVC_{INT}), HVC_{RA} neurons projecting to the robust nucleus of arcopallium (RA) of the motor pathway, and HVC_X neurons projecting to Area X (Daou et al. 2013, Daou and Margoliash 2020).*

Numerous *in vivo* and *in vitro* intracellular recording studies of HVC neurons have been carried out (Katz and Gurney 1981, Lewicki and Konishi 1995, Lewicki 1996, Dutar et al. 1998, Kubota and Taniguchi 1998, Schmidt and Perkel 1998, Mooney 2000, Mooney, Hoese et al. 2001, Mooney and Prather 2005, Solis and Perkel 2005, Wild, Williams et al. 2005, Long, Jin et al. 2010, Shea, Koch et al. 2010, Daou et al. 2013, Daou and Margoliash 2020). These studies shed light on several neuronal and circuit mechanisms and unveiled a variety of physiological properties within the HVC. Only one study however (Daou et al. 2013) took the first step in identifying the ionic currents ingredients of HVC neurons that orchestrate their firing patterns. This was

obtained via whole cell current-clamp recordings from neurons within HVC brain slices to determine which ionic currents are responsible for their characteristic firing patterns. Daou et al (2013) also developed single-compartment conductance-based models for the HVC neurons based on the identified ionic currents and their reported characteristics and then calibrated the models using data from their brain slice work. While this result was an improved characterization of the HVC neurons responsible for singing in the songbird, this single compartment model failed to capture all of the essential features of HVC neurons' spike patterns, leaving the story far from unfinished (Daou et al. 2013).

CHAPTER II

LITERATURE REVIEW

A. Electrophysiological properties of HVC neurons

A very helpful way to decipher the HVC code is to understand how HVC neurons respond when the neurons are stimulated with a patch pipette. We will be summarizing next the characteristic patterns of the three classes of HVC neurons.

HVC_{RA}, HVC_{X} and HVC_{INT} neurons show different firing properties *in vitro*. HVCx neurons have two identifying features in response to applied current. The first feature is the spike frequency adaptation observed in response to depolarizing current pulses (Fig. 2A). The second feature is the moderate sag elicited in response to hyperpolarizing current pulses, followed by rebound firing at the offset of the current pulse (Fig. 2B). Also, this study showed that as the hyperpolarization current pulses were increasing the sag and rebound were larger which is similar to other previous studies (Dutar et al. 1998, Kubota and Taniguchi 1998). Spontaneous firing was also assessed in these neurons, and it was exhibited in a subset of HVCx neurons but abolished after applying AMPA/kainate receptor antagonist CNQX and the $GABA_A$ receptor antagonist PTX.

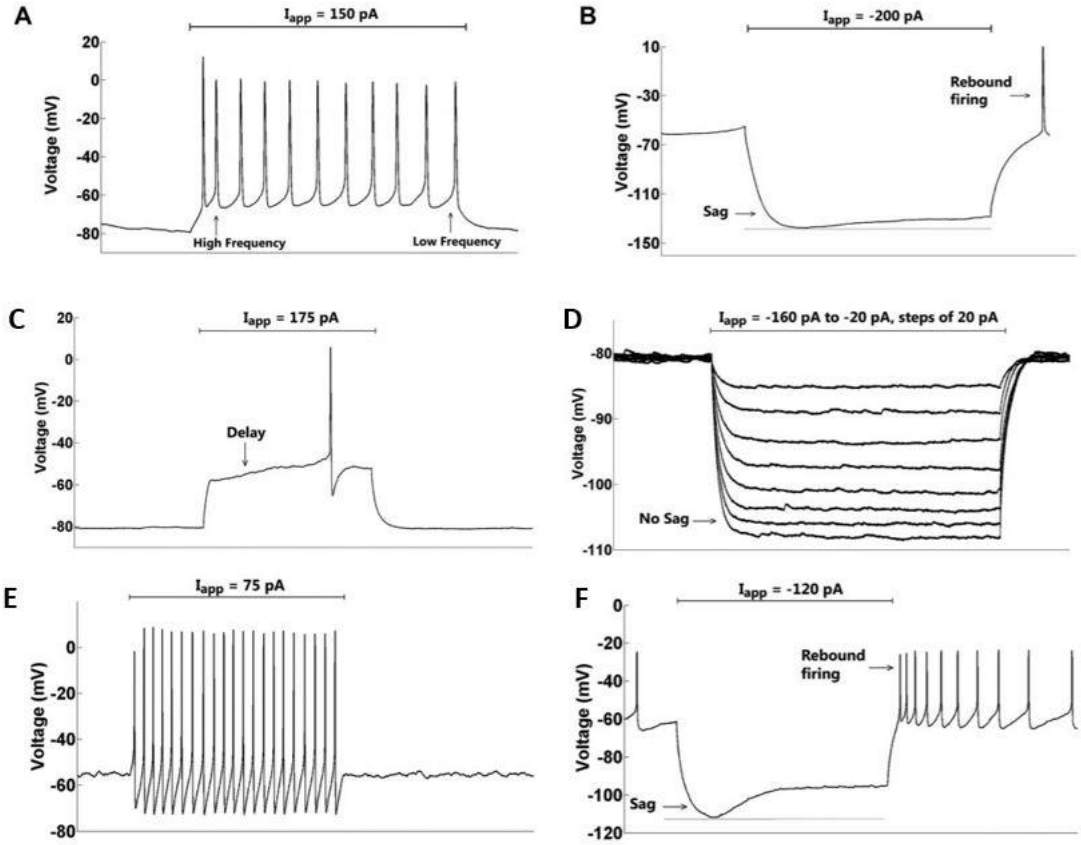

Figure 2*: Biological recordings of HVC neurons.* ***A****: A sample X-projecting neuron exhibiting some spike frequency adaptation in response to a depolarizing current pulse (applied current Iapp = 150 pA).* ***B****: A weak sag followed by postinhibitory rebound firing is generated in response to a hyperpolarizing current pulse (-200 pA).* ***C****: An RA-projecting neuron fires a single action potential, often with a long delay, in response to a relatively large depolarizing pulse (175 pA).* ***D****: No sag is present in response to hyperpolarizing current pulses (-160 to -20 pA, in steps of 20 pA).* ***E****: An HVC interneuron fires tonically at high frequencies in response to a depolarizing current pulse (75 pA).* ***F****: A prominent sag followed by postinhibitory rebound firing is generated in response to a hyperpolarizing current pulse (-120 pA) (Daou et al. 2013).*

Pharmacological blockers were used on HVC_X neurons to assess the ionic currents compositions that these neurons exhibit and that are responsible for their characteristic patterns (Daou et al. 2013). The spike frequency adaptation feature was reminiscent of a Ca^{2+}-dependent K^+ current, and indeed when Apamin was used to block I_{SK} current, the adaptation was gone to large extent (the residual adaptation was

due to the Na^+-dependent K^+ current, I_{KNa}).. . As a result, it was suggested that the after-hyperpolarization (AHP) of HVCx neurons are due to the SK current. Furthermore, the sag and post-inhibitory rebound were examined in order to assess their pharmacological nature. When Mibefradil (a T-type Ca^{2+} current blocker) was bathed to the brain slice, the sag was kept intact but the rebound firing was eliminated suggesting the T-type current as the main player in rebound firing. Meanwhile, the application of ZD 7288 (a hyperpolarization activated inward current blocker) eliminated the sag totally (suggesting I_h as the main player in this mechanism) and the rebound depolarization as well suggesting that rebound firing needs low-threshold T-type Ca^{2+} current as well as I_h in HVCx neurons (Daou et al. 2013).

HVC_{RA} neurons on the other hand has three identifying features that represent their activity (Daou et al. 2013). The first feature revealed that HVC_{RA} neurons have lack of excitability in response to depolarizing current pulses and this was concluded when neurons fired only few spikes, often with a long delay to first spike, after the application of large depolarizing pulses (Fig. 2B). The second feature is the absence of both sag and rebound firing in response to hyperpolarizing current pulses and after its termination (Fig. 2C). Meanwhile, the spacing between spikes becomes smaller with greater hyperpolarizing currents which indicates that there is a fast-inward rectification. Finally, the extremely hyperpolarized resting membrane potential of around -85 mV is the third identifying feature for this class of neurons (Dutar et al. 1998, Kubota and Taniguchi 1998, Daou et al. 2013).

Pharmacological tests showed that SK current plays a key role in damping the excitability of this type of neurons, because the application of Apamin increased the neuron's excitability, decreased the spike amplitude, and depolarized the resting

membrane potential by around 5 mV (Daou et al. 2013). Moreover, the delay to spiking was shown to be due to the A-type K^+ current, because it was blocked by4-AP (4-AminoPyridine, a selective drug for I_A). 4-AP also resulted in increasing the neuron's firing frequency It is important to mention that this class of neurons exhibit frequent spontaneous depolarizing synaptic potentials as well as it has a low input resistance (Dutar et al. 1998). Additionally, HVCRA neurons have large AHP amplitude and a short time-to-peak duration (Dutar et al. 1998, Daou et al. 2013).

Finally, HVC interneurons are the third known class of neurons in HVC and they have two identifying features (Daou et al. 2013). The first feature is the high firing frequency in response to a relatively small depolarizing pulses (Fig. 2E), and this had been seen in different studies (Dutar et al. 1998, Kubota and Taniguchi 1998, Daou et al. 2013). The second identifying feature for this class of neurons is the presence of a very prominent sag as well as strong rebound firing in response to hyperpolarizing current pulses after its termination (Fig. 2F) (Daou et al. 2013). The sag and the rebound firing observed in HVCINT neurons were shown to be due to the hyperpolarization activated inward current Ih and the T-type Ca^{2+} current, respectively (Daou et al. 2013). Equally importantly, this class of neurons do not express an SK current as they do not exhibit any form of adaptation.

This type of neurons also has a significantly longer action-potential (Dutar et al. 1998), resting membrane potential of around −67.6 mV (Dutar et al. 1998), large-amplitude AHP with a short time-to-peak duration (Dutar et al. 1998, Daou et al. 2013).

Beside the classification of HVC neurons based on their ionic channels, HVC neurons have been stratified into four classes (I, IIa, IIb, III and IV) based on their different electrophysiological and morphological properties (Dutar et al. 1998, Kubota

and Taniguchi 1998). Type I neurons were found to have large somata accompanied by spiny thick dendrites; most of them project to Area X. Type II neurons have been divided into two subclasses: neurons IIa have small somata and thin dendrites, while neurons IIb are characterized by their relatively large somata and thick dendrites. Type IIa neurons show similar electrical properties to HVC_{RA} neurons. Furthermore, type III neurons have beaded dendrites and exhibit tonic firing with almost no adaptation, reminiscent of HVC interneurons. Finally, type IV neurons exhibit very small somata, as well as thin, short and spiny dendrites. Some of these neurons project to RA (Kubota and Taniguchi 1998).

B. Intrinsic plasticity of HVC neurons

To understand how function emerges from ensembles of neurons and their interactions, we need a rigorous interplay of theoretical work and experimental approaches capable of listening to the activity of neurons and relating cellular properties to behavior. This synergy of theory and neurophysiology is beautifully illustrated in recent work by Daou and Margoliash (2020) that studied the intrinsic properties of a large population of HVC_X neurons. They report a surprising mechanism that stores information about song structure rapidly. By analyzing the raw data traces in response to somatic current injections, they showed a consistent pattern of homogeneity of HVC_X intrinsic properties within individual adult birds and variation among birds related to the birds' songs. The homogeneity is maintained by plastic mechanisms and is sensitive to auditory perturbations. In particular, the spiking patterns for the HVC_X neurons of a specific bird tended to have similar onsets, numbers of spikes, and timing of spikes, whereas these characteristics varied from one bird to another. Such

uniformity within individual animals was not known and was unanticipated given the variation within individual birds in the spiking patterns of different HVC_X observed during singing.

In addition to the uniformity in spikes timing among HVC_X neurons in the same bird, the spike waveforms (morphologies) of the HVC_X also tended to conform to a common shape for a given bird, while spike shape varied from bird to bird. In particular, intrinsic properties like plateau amplitude, spike amplitude, spike threshold, and inter-spike interval (among many others) are almost the same in a specific bird and varies a lot across different birds as shown in Fig. 3. These properties were shown to be due to purely intrinsic mechanisms and not synaptic.

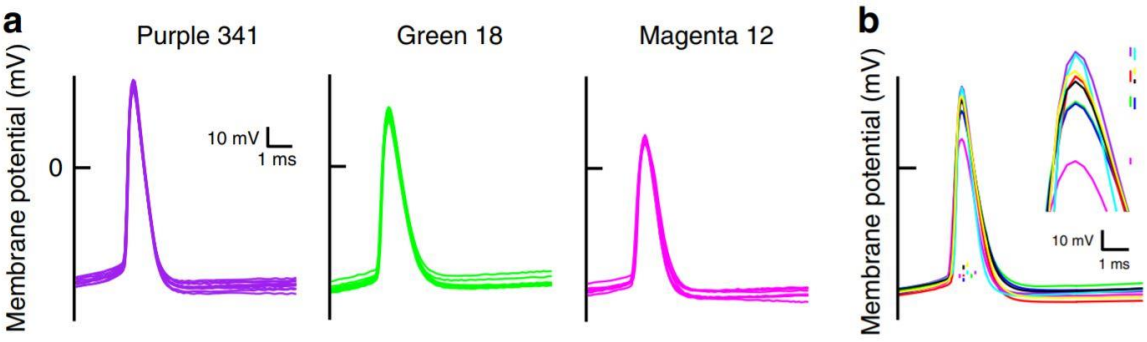

***Figure 3**: Individual birds have uniform and distinct HVC_X intrinsic properties: spike waveforms. The same color is used to represent birds that appear in more than one panel. **a**: The first spike waveforms have similar shape within each bird (Purple 341, 10 HVC_X; Green 18, 9 HVC_X; Magenta 12, 8 HVC_X), and spike shapes differ across the birds. **b**: The averaged first spike waveforms for each of the eight birds with the greatest numbers of HVC_X recorded. Each bird is represented by a different color. Vertical bars are centered on the spike threshold values, with the height of the bars representing the spike threshold variability (±1 SD). The bars are slightly offset from each other to improve visibility. Inset shows detail of average spike waveforms near their peaks. The vertical bars are centered on the peak of the average spike amplitudes, with the height of the bar representing the amplitude variability (±1 SD) (Daou and Margoliash 2020).*

Daou and Margoliash (2020) then explored the relation between HVC_X dynamics and spike shape by modeling the magnitude of ion currents in a large subset

of the neurons based on an already established model (Daou et al. 2013). Examining the distribution of predicted current magnitudes (manual fitting) for the five ion channels in HVC_X revealed that the neurons from each animal occupied a small volume in the five-dimensional space of ion conductance magnitudes, and that there were large differences between animals (Figure 4). More importantly, this homogeneity in ionic conductances was tightly correlated to features of song (pitch, amplitude, entropy…), such that birds that exhibit similar songs exhibit as well similar distributions of ionic currents (Daou and Margoliash 2020). It's the first result that relates cellular properties (ion channels) to behavior (song), and it shows to the extent understanding the intrinsic properties of neurons is important to understanding fundamental mechanisms of the brain that underlies learning and memory.

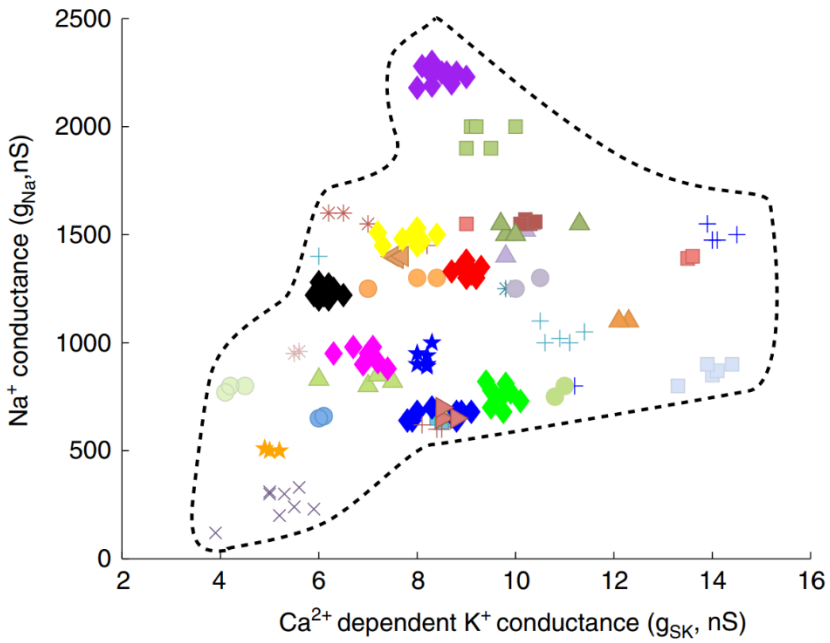

Figure 4: *A scatter plot of all 151 manually modeled neurons showing the two conductances that varied the most across the population, g_{Na} and g_{SK}. Different animals (N = 38), denoted by different color symbols, occupy different regions in the 2D space. The dashed line encloses the 2D conductance space of the modeled data set, representing an estimate of the entire parameter space occupied by the population of normal adult zebra finches (Daou and Margoliash 2020).*

C. Mathematical modeling of HVCx neurons

Each HVC neuronal population has different functional properties and ion channels composition responsible for various responses to depolarizing and hyperpolarizing stimuli. Ionic channels for each neuron type were previously identified using chemical blockers (Daou et al. 2013). In their work, Daou et al (2013) also developed a biophysically realistic model that was tuned to fit the biological data they generated *in vitro*, incorporating the ionic currents that were identified pharmacologically. The Daou et al 2013 model incorporated the potassium (I_K) and sodium (I_{Na}) currents as spike generating currents, a high threshold L type calcium current (I_{CaL}), a low threshold T type calcium current (I_{CaT}), a small conductance calcium activated potassium current (I_{SK}), a persistent sodium current (I_{Nap}), a sodium dependent potassium current (I_{KNa}), an A type potassium current (I_A), a hyperpolarization activated inward current (I_h) and a leak current (I_L). These currents were shown to be the main players in orchestrating the HVC neuronal firing patterns (Daou et al. 2013).

The membrane potential of every HVC neuron obeys the following equation:

$$C_m \frac{dV}{dt} = I_{app} - I_{Na} - I_K - I_A - I_h - I_{SK} - I_{KNa} - I_{Nap} - I_{CaL} - I_{CaT} - I_L$$

where C_m is the membrane capacitance and I_{app} the magnitude of the applied current.

While all model neurons share the same ionic currents, there are some differences however in the ionic currents' magnitudes across the three classes of HVC neurons For example, HVC interneurons that lack the adaptation feature have a very small I_{SK} and I_{KNa} currents, while in return they exhibit a much stronger I_K and

I_h currents than the other two classes of projecting neurons. RA-projecting neurons seem to be the only class of neurons that exhibit a strong A-type K^+ conductance due to the delay to first spike feature that they exhibit solely. Moreover, X-projecting and interneurons are the only neurons that exhibit I_h and I_{CaT} currents because they are the only neurons that exhibit a sag and rebound firing in response to negative current pulses. The model responses and fits are shown in Fig. 5.

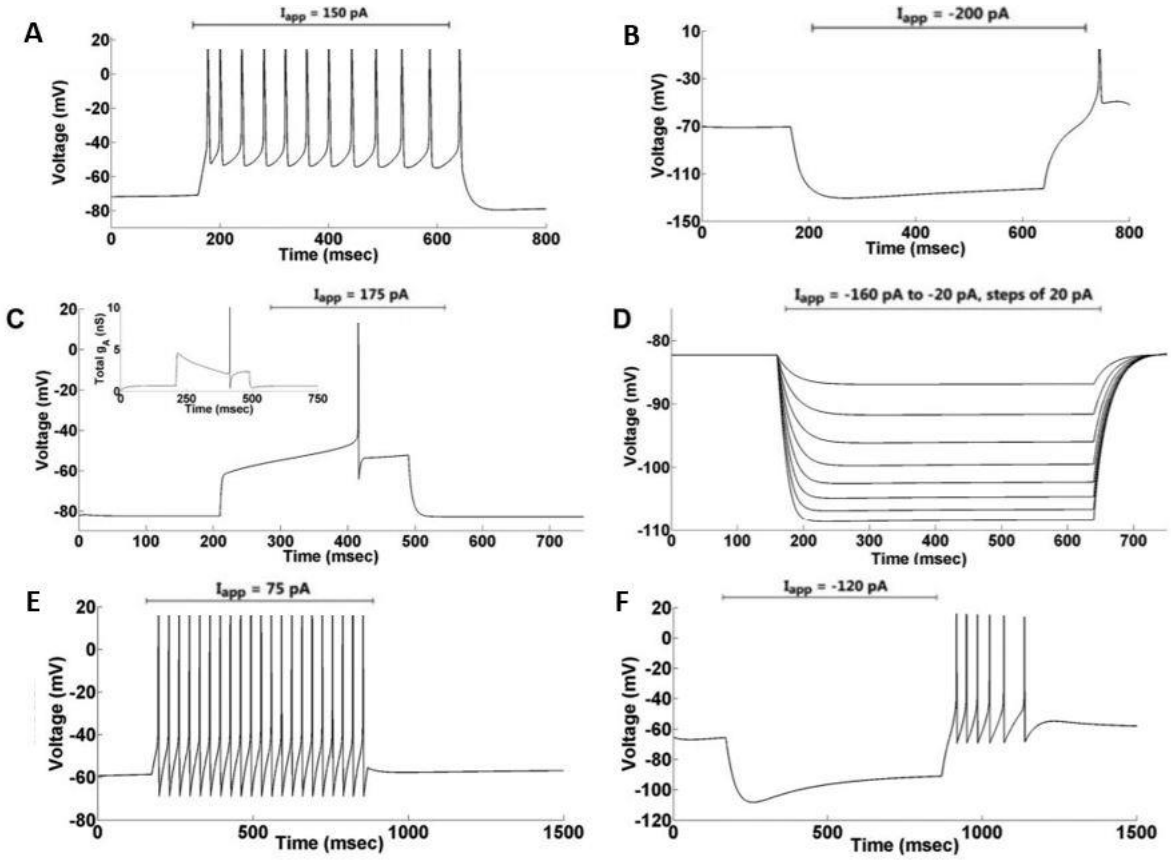

Figure 5: *Model simulations for HVC neurons.* ***A*** *and* ***B****: HVC_X model neuron parameters were calibrated to match the voltage traces (Fig.* ***2A*** *-* ***2B****). The same magnitude of applied currents used in the slice was used in the model simulations in this figure.* ***C****: HVC_{RA} model neuron parameters were calibrated to match the experimental recording (I_{app}= 150 pA). The long delay to spiking is due to the A-type K^+ current (I_A). Inset shows the total I_A conductance (g_A) during the current pulse.* ***D****: For the same parameter values used in* ***C****, the HVC_{RA} model neuron has no sag but exhibits inward rectification in the spacing between voltage traces, as in (Fig.* ***2D****). E and F: HVC_{INT} model neuron parameters were calibrated to match the voltage traces (Fig.* ***2E*** *-* ***2F****) to positive and negative current pulses respectively (Daou et al. 2013).*

Several modeling frameworks have tried to describe the firing patterning of HVC neurons. Gibb et al. 2009 was the first to develop a computational model of HVC neurons. Their model, though non-biologically realistic, hypothesized for the first time that different networks in HVC control different syllables production, that HVC_{INT} provide mutual inhibition between networks controlling syllables, and that these syllable networks are sequentially excited by neural feedback via the brain stem or a similar feedback pathway (Gibb et al. 2009). In a subsequent work, they showed that the sparse bursting seen in projecting neurons is generated in bistable groups of recurrently connected HVC_{RA} neurons with the inhibitory interneurons terminating bursts in the HVC_{RA} groups (Gibb et al. 2009).

Other models of how HVC neurons might be organized and interconnected have been proposed (Troyer and Doupe 2000, Drew and Abbott 2003, Abarbanel, Gibb et al. 2004, Abarbanel, Talathi et al. 2004, Mooney and Prather 2005, Li and Greenside 2006, Jin 2009, Long, Jin et al. 2010), but all of these models have failed to capture the intricate details of spike morphology, failed to incorporate the right ionic currents that exist biologically, or failed to generate the same patterns seen *in vivo*.

None of the above mentioned research projects created a model that can replicate the neurophysiological firing patterns and properties seen in the HVC_X neurons of the zebra finch. However, some tried to model HVC_{RA} and HVC_{INT} neurons as the one used by Gibb et al. 2009, where their models was able to generate sparse bursting based on inhibition, recurrent excitation, and bistability.

Another example is the model of Jin 2009, where they modeled HVC_{RA} as a two-compartment model attributing the HVC_{RA} bursts to an intrinsic cellular mechanism located in the dendrite. This work showed that dendritic spike enhances the

stability of burst propagation in chain network, and variable syllable sequences can be generated within HVC through competitive spike propagations in chain networks of HVC_{RA} neurons connected into branching chain pattern, replicating the exact behavior of HVC_{RA} and HVC_{INT} in the zebra finch. In short, most of the work done on HVC modeling didn't put much effort on HVC_X neurons or discussing their importance in the songbird learning process. This class of neurons is the main focus of this thesis.

CHAPTER III

MATERIAL AND METHODS

A. Brain Slice Electrophysiology

All of the modeled neural traces in this study were collected by the PI at the University of Chicago from HVC_X neurons using the patch clamp technique. In short, birds were anesthetized with isoflurane and rapidly decapitated. The brain was quickly removed and placed in ice-cold artificial cerebrospinal fluid (ACSF) before it was moved to standard NaCl-based ACSF solution for incubation at room temperature (Daou et al. 2013, Daou and Margoliash 2020). Recordings were initiated after 1 h of total incubation. Whole cell patch-clamp recordings from HVC neurons were made with unpolished electrodes filled with intracellular solution. Neurons were applied with a series of current pulses, of different magnitudes (40 pA to 200 pA, steps of 20), and of duration 200 ms.

B. Electrophysiology Single Compartment Modeling

Single-compartment conductance-based biophysical models of cells of of HVC_X neurons were developed, based on the collected current-clamp data. Simulations of these model neurons were performed using MATLAB (MathWorks) and XPPAUT (Pittsburgh). The functional forms of activation/inactivation functions and time constants were based on published neural models (Hodgkin and Huxley 1952, Destexhe and Babloyantz 1993, Meunier and Segev 2002, Terman, Rubin et al. 2002, Wang, Liu et al. 2003, Daou et al. 2013), and the majority of our fitting parameters were maximum

conductances and activation/inactivation kinetics, which are likely to vary among cell types.

We created a single compartment conductance-based model using Hodgkin Huxley (H-H) mathematical equations, because they form the fundamental framework for understanding the spike propagation in axons, hence studying neuronal excitability and all its features (Meunier and Segev 2002). Two-compartment models in theory are more accurate but there is no biological data collected in our lab or any other lab that describes how the dendritic or axonic departments function in these neurons. Activation and inactivation of voltage dependent currents during different time frames are examples of some features that are vital to be explored and applicable to be studied using this model. Also, the differential equations of H-H model permit the capturing of biophysical systems (neurons) that are based on nonlinear properties. Moreover, different neuronal firing features such as bursting, resonance, adaptation are few among many other features that can explored in our model and that could reveal the geometry of excitability and morphology of spikes. Phase plane analysis which is important to learn more about stability, bifurcation, and the overall geometric nature of the solutions are conducted as well (Meunier and Segev 2002).

In this model, the somatic ionic currents were previously tested and verified in the brain slices (Daou et al. 2013) by pharmacological manipulations. We took in this work a minimalistic approach to modeling the neurons to understand the fundamental backbones of the model as follows: The Na^+-dependent K^+ current that was in the Daou et al (2013) model was not included in our model because there was no *selective* pharmacological blocker for that current in that study, leaving the expression of this current unclear. The T-type Ca^{2+} current and the hyperpolarization activated inward

current are two currents that have little to no influence on the spike dynamics when the neurons are stimulated with depolarizing current pulses, as they operate more in the negative regime when neurons are given negative current pulses. Since we are basing our modeling on positive current pulses, we excluded these two currents from our model. The following equation describe the transmembrane potential of the used model:

$$C\frac{dV}{dt} = I_{app} - I_{Na} - I_K - I_{SK} - I_{CaL} - I_L$$

where C is the membrane capacitance and I_{app} is the current applied.

This soma compartment contains: sodium current (I_{Na}), potassium current (I_K), Ca-activated K current (I_{SK}), L-type calcium current (I_{CaL}), and the leak current (I_L). The equations used for Na^+ and K^+ equations and currents are:

$$m_\infty = \frac{1}{1 + e^{\frac{v-\theta_M}{\sigma_M}}}$$

$$n_\infty = \frac{1}{1 + e^{\frac{v-\theta_N}{\sigma_N}}}$$

$$\tau_N = \frac{\tau_{\bar{N}}}{cosh\left(\frac{(\mathrm{v} - \theta_N)}{(2 \times \sigma_N)}\right)}$$

$$\alpha_H = \alpha_1 \times e^{-\frac{v+\alpha_2}{\alpha_3}}$$

$$\beta_H = \frac{\beta_1}{1 + e^{-\frac{v+\beta_2}{\beta_3}}}$$

$$h_\infty = \frac{\alpha_H}{\alpha_H + \beta_H}$$

$$I_{Na} = g_{Na} \times {m_\infty}^3 \times h \times (v - v_{Na})$$

$$I_K = g_K \times n^4 \times (v - v_K)$$

The equations used for L-Type Ca^{++} equations and current are:

$$s_\infty = \frac{1}{1 + e^{\frac{v-\theta_S}{\sigma_S}}}$$

$$I_{Ca} = g_{Ca} \times {s_\infty}^2 \times v \times \frac{Ca_{ex}}{1 - e^{\frac{2\times v}{RTF}}}$$

The equations used for T-Type Ca2+ equations and current are:

$$aT_\infty = \frac{1}{1 + e^{\frac{v-\theta_{aT}}{\sigma_{aT}}}}$$

$$bT_\infty = \frac{1}{1 + e^{\frac{rT-\theta_{bT}}{\sigma_{bT}}}} - \frac{1}{1 + e^{-\frac{\theta_{bT}}{\sigma_{bT}}}}$$

$$rT_\infty = \frac{1}{1 + e^{\frac{v-\theta_{rT}}{\sigma_{rT}}}}$$

$$\tau_{rT} = \tau_{r0} + \frac{\tau_{r1}}{1 + e^{\frac{v-\theta_{rT}}{\sigma_{rT}}}}$$

$$I_T = g_T \times {aT_\infty}^3 \times {bT_\infty}^3 \times v \times \frac{Ca_{ex}}{1 - e^{\frac{2\times v}{RTF}}}$$

The equations used for SK equations and current are:

$$k_\infty = \frac{ca^2}{ca^2 + ks^2}$$

$$I_{SK} = g_{SK} \times k_\infty \times (v - v_K)$$

The equation used for Leak current is:

$$I_L = g_L \times (v - v_L)$$

All the differential equations in the model are simulated using two built-in software MATLAB and XPP. XPP will be primarily used for dynamical systems applications of this work, like generating bifurcation diagrams of some key parameters, fine tuning of others, etc.… In order to fit the model in the most accurate way to the biological recordings, error functions were designed that captures the difference in spike heuristics between the biological and model simulations (both actual spikes morphology and spikes timing). The aim is to minimize this error utilizing a brute force search on some key parameters in the model. The error function used mean squares to compute the difference between the biological voltage trace and the model simulation by adding the individual differences between the two for each of the following features: plateau amplitude, spike amplitude, spike duration, number of spikes, the timing of each individual spike, and resting membrane potential. These features were only well defined for the responses to step current pulses.

We started applying the above methods and functions by overlaying both biological and model traces and adjusting the parameters to have same number of spikes acceptable fits. Then we extracted the first spike waveforms of both traces and overlaid them peak to peak in order to calculate the mean square error between them. The following step was conducted to unveil the most important parameters that controls these waveforms, study their effect on the spike's morphology and get the optimal

value or magnitude for each parameter that controls their dynamics. Finally, we used the optimal values for all parameters that are elicited by the error functions. This process was repeated for 30 neurons from 4 different birds.

The aim of this study is to unveil more information at the cellular level that would enable us to create more realistic models that better approaches the neural networks level. Since there is a tight relation between the neuronal ion channels and the neuronal encoding schemes (Wang, Wang et al. 2013, Yi, Wang et al. 2014), designing a model with the accurate ionic currents' parameters is a very key step in the process. However, this turns out to be one of the toughest questions in the field due to the high complexity and nonlinearity it exhibits, the high variations in output patterns, and the large number of unknown variables. Therefore, we found it a necessity to tackle this area in our study because translating this bottom-up approach will allow much understanding of the biophysical properties of HVC neurons, have more insights about the neural encoding of this nucleus (Yi, Wang et al. 2014), and in turn contribute to discovering how HVC neurons encode song.

CHAPTER IV

RESULTS AND DISCUSSION

HVC_X neurons emit adapting spike trains in slice when stimulated by somatic current injections. In response to injections of the canonical depolarizing currents, the spike patterns for HVC_X neurons from different birds tended to have different onsets, numbers of spikes, and timing of spikes (Fig. 6A) while these properties are similar within the same bird (Daou and Margoliash 2020). For example, among the eight overlaid neurons in Fig. 6A, the black colored trace has 4 spikes with around 50ms first interspike interval, while blue colored trace has 6 spikes with 40ms first interspike interval.

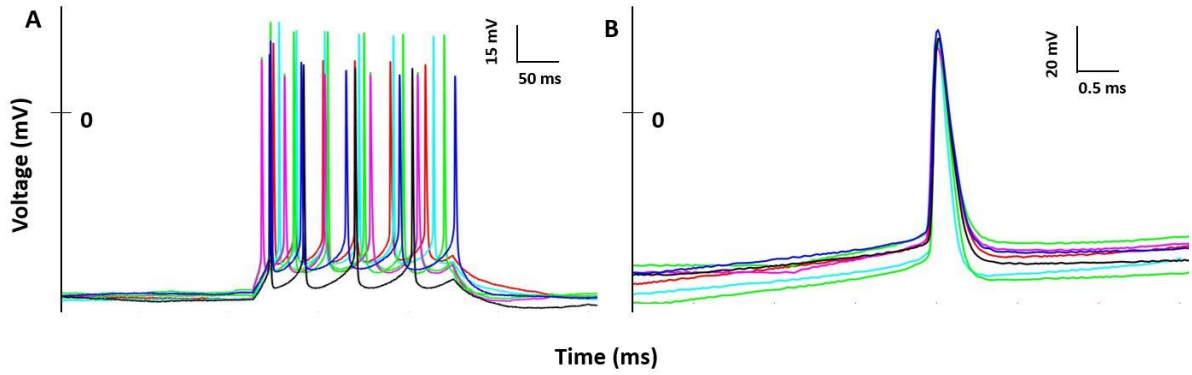

***Figure 6**: Heterogeneity across the various biological recordings. **A**: Overlaid biological recordings for HVC_X neurons from 7 different birds. **B**: Overlaid first spike morphology for HVC_X neurons from 7 different birds. Both A and B panels show the differences in spike trains and morphology from one HVC_X neuron to another.*

The waveforms for the individual spikes of the HVC_X also tended to vary from bird to bird. In particular, the spike width, threshold, plateau amplitude, input

resistance, after-hyperpolarization (AHP), upstroke and downstroke of the action potentials differ across these neurons (Fig. 6B). As an example, the range of amplitudes for these eight neurons varied from a minimum of 85 mV (purple trace) to a maximum of 110 mV (green trace). Therefore, the intrinsic features that HVC_X neurons exhibit vary from one bird to another, and even though these recordings are from the same class of neurons, from the same brain area, and from the same species, each neuron tended to exhibit its own behavior and unique characteristics when recorded from different birds.

The relation between neuronal dynamics and spike shape should be influenced by the magnitude of ion currents of the given cell. We started by exploring the relationship between HVC_X neurons' dynamics and the spike shape by fitting the biological traces to the model. Cells were modeled with a charge balance equation of the Hodgkin–Huxley type (see Methods), using an HH model incorporating ion currents that have recently been pharmacologically demonstrated for HVC_X. While understanding the overall behavior of an HVCx neurons is a vital step in modeling, understanding the role and function of each parameter mentioned in the previous studies in the literature will allow us to model properly and in an efficient way. Therefore, we started our tuning process where we tested all the given parameters on MATLAB and XPPAUT to check the model response and to find the accepted ranges.

We were mostly interested in matching the timing of individual spikes as well as the first spikes' morphology, incurring penalties on any mismatch in these two domains (see Methods). By varying each of the parameters in our model, we were able to figure out the most significant parameters in our model that orchestrate the aforementioned intrinsic features. While the Ca^{2+}-dependent K^+ current and the L-type

Ca^{2+} current play significant roles in shaping the timing of spikes, they play little role in individual spikes shapes. So, we focused our attention at the voltage-dependent Na^+ and K^+ currents that play most of the role in shaping the upstroke and downstroke spikes morphologies.

Figure 7 shows the model responses to the 9 key parameters in the Na^+ and K^+ equations that were used to fit the biological spike for a sample neuron. Each one of these parameters showed a significant role in changing the morphology of the action potentials. In this and subsequent panels, red traces represent spikes for ranges of the parameter that generated minimal error function values (that is, the range of best fits for that parameter), while black traces represent spikes for ranges of the parameter that generated bad fits, and the blue trace represent the biological trace. All parameters were varied across biologically realistic domains. Panels A to D shows the response of the model over the biophysically realistic ranges of α_2, β_1, β_2, and β_3 respectively (parameters and equations shown in Methods). As shown, varying the parameter β_1 and β_3 (Fig. 7B, 7D) will have drastic effects on the spike's width, spike's amplitude, spike's threshold and the overall morphology, while varying parameters α_2 and β_2 show only little effects to the upstroke with minimal changes on the rest of the spike waveform (Fig. 7A, 7C). In addition, half-activation parameters for Na^+ and K^+ currents have a big impact on spike morphology and spike rate, where θ_M (Fig. 7F), σ_M (Fig. 7I), θ_N (Fig. 7G) and σ_N (Fig. 7H) affect the number of action potentials, spike amplitudes, and the repolarization of the spikes' train (mainly AHP region). Finally, the maximal conductances g_{Na} and g_K controls primarily the velocity of the upstrokes and downstrokes respectively, thereby controlling indirectly the spike amplitude, spike width and the after-hyperpolarizing regions (AHP).

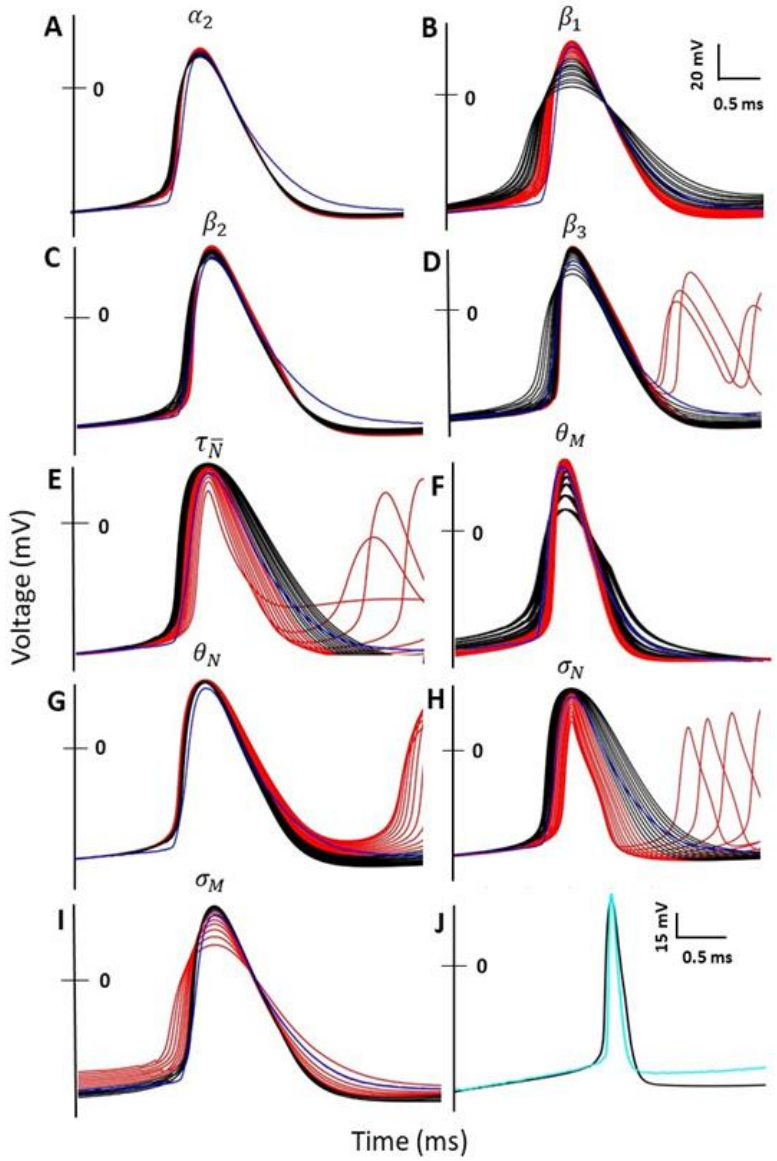

Figure 7*: Tuning of Na^+ and K^+ parameters to match the biological spikes. Red traces represent spikes for ranges of the parameter that generated minimal error function values (that is, the range of best fits for that parameter), while black traces represent spikes for ranges of the parameter that generated bad fits, and the blue trace represent the biological trace.* ***A****: Tuning over different values for α_2 (red: 48 to 53 & black: 53.5 to 58) with a step size of 0.5.* ***B****: Different values for β_1 (red: 2 to 4 & black: 4.2 to 6) with a step size of 0.2.* ***C****: Different values for β_2 (red: 22 to 25 & black: 25.5 to 29) with a step size of 0.5.* ***D****: Different values for β_3 (red:1 to 3 & black: 3.2 to 6) with a step size of 0.2. .* ***E****: Different values for $\tau_{\bar{N}}$ (red: 1 to 10 & black: 10.5 to 20) with a step size of 0.5.* ***F****: Different values for θ_M (black: -34 to -36 & red: -36.5 to -38) with a step size of 0.5.* ***G****: Different values for θ_N (red: -15 to -20 & black: -20.5 to -25) with a step size of 0.5.* ***H****: Different values for σ_N (red: -4 to -9 & black: -9.5 to -14) with a step size of 0.5.* ***I****: Different values for σ_M (red: -5 to -8 & black: -8.5 to -11) with a step size of 0.5.* ***J****: The biological trace (light blue) overlaid with the model trace (black) after substituting the optimal values taken from the analysis of the previous parameters.*

Varying these parameters in different combinations will also likely to have combinatory positive and negative effects on the goodness of the fit, yet this will necessarily increase the nonlinearity of the problem and we'll be considering it in our next step in this research. However, through the careful analysis of these parameters and the exact effects or roles each parameter plays, we were able to reach to suboptimal values that were able to generate better fits. Figure 7J shows such an optimal response for the same modeled neuron in panels (7A-7I) where the model was able to capture much of the intricate details of the first spike morphology where other models failed previously to do so. While the model simulation still doesn't match the first spike morphology 100%, it generates a better fit than what is previously reported (Daou et al. 2013).

We then used a supercomputer at the University of Chicago (Cray XE-6, 24k cores) as well as at MSFEA (Octopus cluster with extra 48 workers on MATLAB clusters) to conduct exhaustive parameter searches on the space of our parameters to check for a better optimal fit over the same ranges and the same parameters. We used the error function described above to compare model and biological traces. Any model simulation that generated a spike train exhibiting different numbers of spikes than the biological trace was disregarded prior to computing the error. The exhaustive parameter searches generated unrealistic spike morphologies (Fig. 8), implicating inadequacies in the error function. The main goal of the parameter searches was to test the validity of the manual fit estimates. The manual fit, however, elicited a more realistic looking trace when compared with the biological recording in terms of its plateau amplitude and the smooth AHP following action potentials (Fig. 8A-8B). The discrepancies between the two is largely due to limitations in the way the error function was constructed. Because

the computed error is a summation of the difference between the model simulation and the biological recording from each of the extracted features, the minimum does not always represent the most optimal solution, although it matches one or more of these features better.

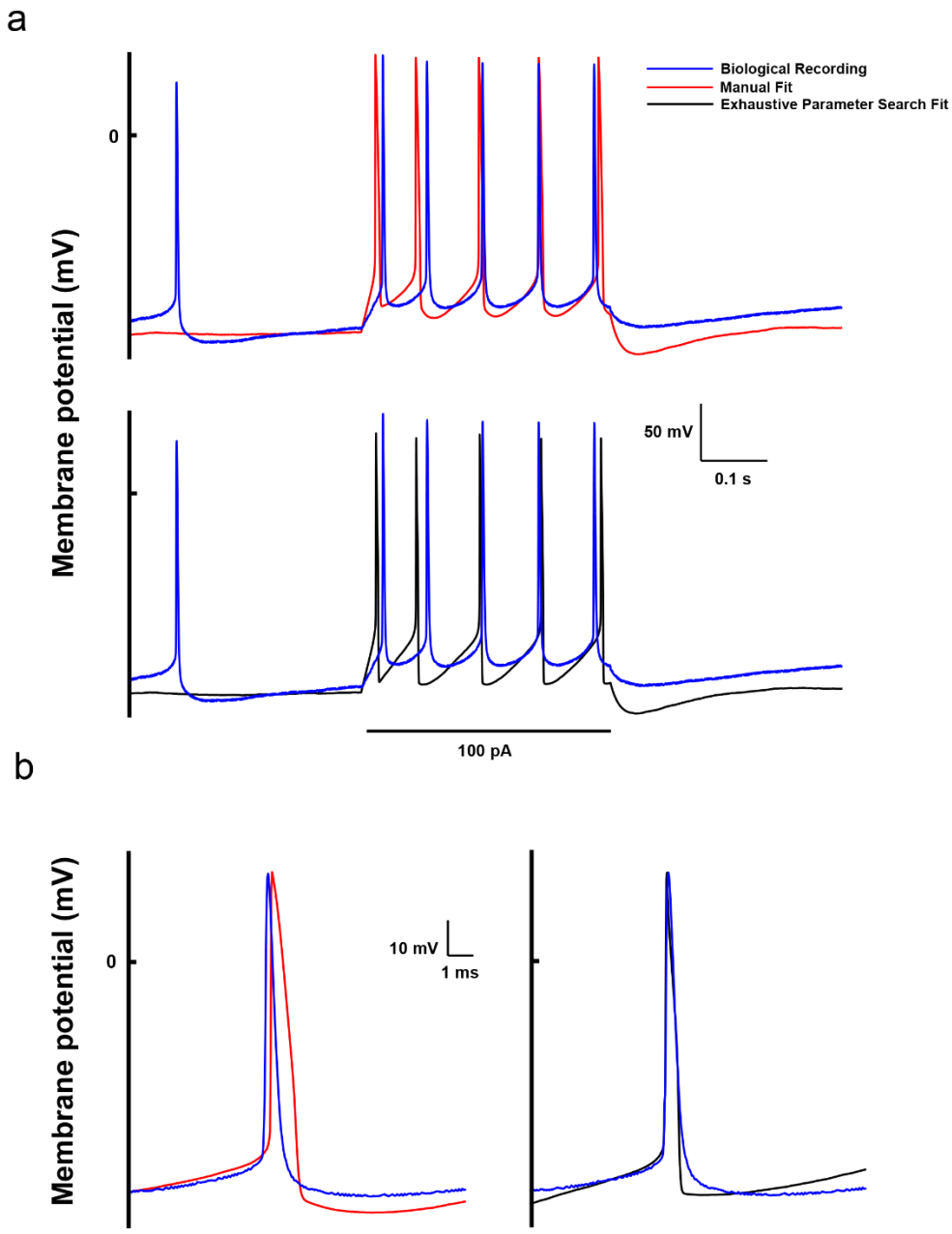

***Figure 8**: Brute force search results. A: Comparison of manual and automated fits illustrating the biological discrepancies of the brute force search results. B: Peak to peak spike waveform of both manual and automated fits.*

We then conducted this fitting paradigm on a subset of experimentally collected HVC_X neurons to assess to what extent the model can replicate different neurons with relatively different firing patterns and to check whether the parameters of the Na^+ and K^+ currents that reflect their activation kinetics vary across birds in a lawful manner similar to what had been reported in Daou and Margoliash (2020). We did this analysis for 30 neurons in 4 distinct birds (Black 111, Red 240, Yellow 15, and Cyan 12) that were collected in the Daou and Margoliash (2020) paper. Similar to what's shown in Fig. 7, the parameter kinetics for the Na^+ and K^+ currents were varied over biologically realistic domains (Table 1).

	From	*To*	*Step Size*
g_{Na}	350	650	50
g_K	120	230	10
g_{SK}	10	28	1
β_1	2	6	0.5
β_2	25	45	2
β_3	1.5	2.5	0.2
$\tau_{\bar{N}}$	6	10	0.5
θ_M	-40	-36.5	0.5
θ_N	-29	-22	0.5
σ_N	-10.5	-8	0.5
σ_M	-8	-5.5	0.5

***Table 1**: Ranges for the 11 different Na^+ and K^+ related parameters that played a crucial role in the fitting of our 30 different neurons.*

Figure 9 shows the response of the model over the biophysically realistic ranges of the associated parameters as shown earlier (Fig. 7) for one sample neuron of bird Red240. With the right tuning of parameters, we are able achieve better fits for the first spike's width, spike's amplitude, spike's threshold and the overall morphology, which are the major bottleneck in this fitting paradigm. Moreover, the number of action potentials, spike amplitudes, and the repolarization of the spikes' train (mainly AHP region) are better restored (Fig. 10), as will be discussed next Therefore, the fast Na^+ and K^+ activation kinetics play the key role in orchestrating the intrinsic details of the first spikes in the spike train of action potentials that HVC_X neurons elicit in response to depolarizing current pulses. Having the right values for these parameters integrated, the model HVC_X neurons are able to generate better predictions of the neuron in response to other stimuli and better fits for spike timing and number of action potentials that are in the spike train. This modeling procedure was conducted for every neuron in our dataset and we collected the parameters for each neuron and in each bird that gives us the best fits.

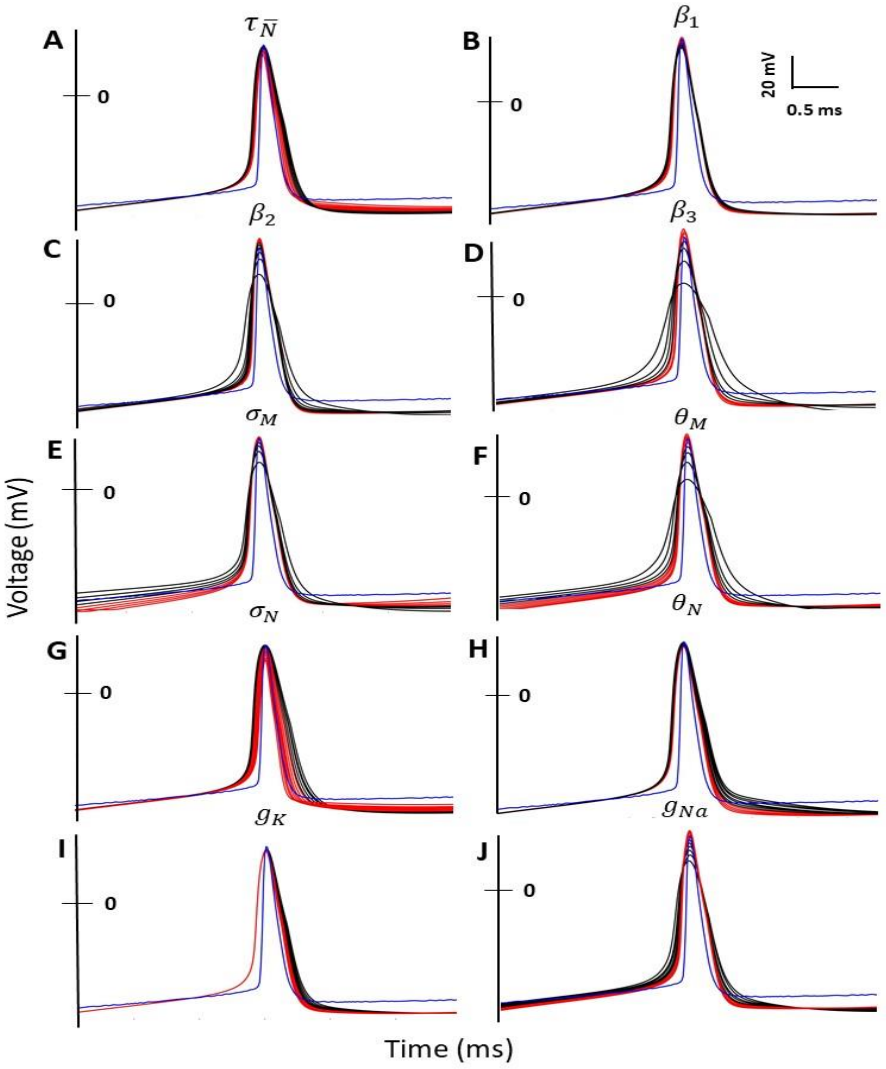

***Figure 9**: : Tuning of Na^+ and K^+ parameters to match the biological spikes for Neuron 3 of Red 240 bird. Red traces represent spikes for ranges of the parameter that generated minimal error function values (that is, the range of best fits for that parameter), while black traces represent spikes for ranges of the parameter that generated bad fits, and the blue trace represent the biological trace. **A**: Tuning over different values for $\tau_{\bar{N}}$ (red: 5 to 10 & black: 10 to 15) with a step size of 1. **B**: Different values for β_1 (red: 2 to 4 & black: 4.5 to 6) with a step size of 0.5. **C**: Different values for β_2 (red: 33 to 37 & black: 38 to 43) with a step size of 1. **D**: Different values for β_3 (red:1 to 1.6 & black: 1.8 to 2.4) with a step size of 0.2. . **E**: Different values for σ_M (red: -12 to -10.5 & black: -10 to -8.5) with a step size of 0.5. **F**: Different values for θ_M (black: -40 to -38 & red: -37.5 to -36) with a step size of 0.5. **G**: Different values for σ_N (red: -12 to -9 & black: -8.5 to -6) with a step size of 0.5. **H**: Different values for θ_N (red: -28 to -23 & black: -22 to -18) with a step size of 1. **I**: Different values for g_K (red: 125 to 185 & black: 200 to 260) with a step size of 15. **J**: Different values for g_{Na} (red: 475 to 600 & black: 625 to 725) with a step size of 25.*

All of the above simulations were computer simulations that allowed us to have optimal ranges and values for all the key parameters, but these optimal values for parameters were solely based on an error function that calculates the mean square error (MSE) between the biological and model traces. However, as discussed earlier (Fig. 8), there are discrepancies between the automated procedures and the manual fitting. So, after we received the optimal fits from the computer simulations, we performed some further manual editing to adjust the morphology of the spikes and/or the whole train in order to have more realistically looking traces. Figure 10 shows the results of the simulations of 5 sample neurons from 4 different birds that show the optimal fitting between the biological traces and the model simulations in both the whole spike trains (left panels) and their corresponding first spike morphologies (right panels). The model was able to capture the spikes' timing efficiently and little less so for their first spike morphologies. Finally, the model was able to obtain a best fit for all the chosen 30 neurons from the 4 different birds and it succeeded in capturing almost all the details of the first spike morphology as well as the spike train firing pattern. This model is the first model in the literature that was able to capture all the intricate details of the first spike morphology along with maintaining the optimal fit for the whole spike train.

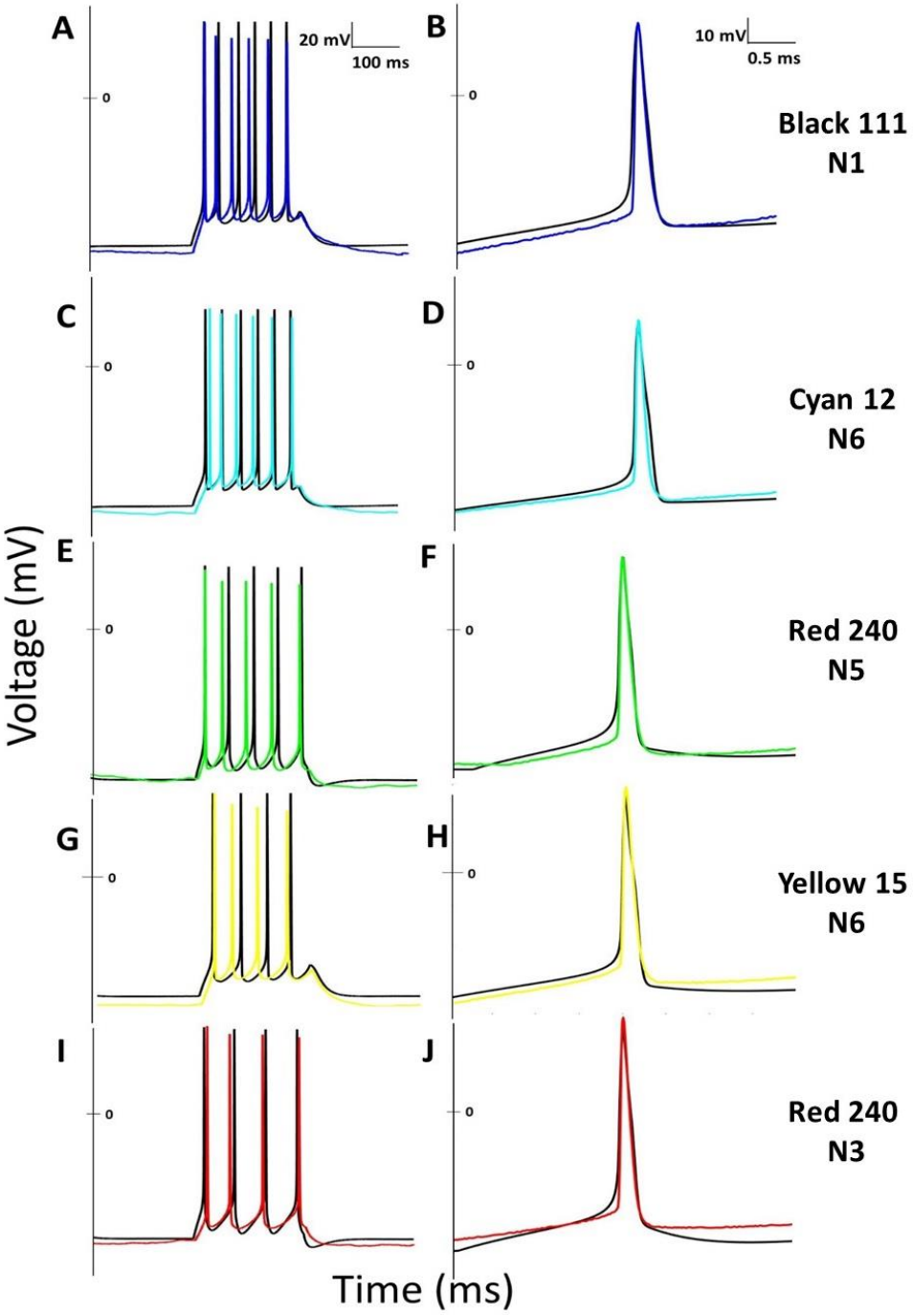

Figure 10*: Simulations and parameters estimations of the model parameters. The spike trains for five different HVC_X neurons from four distinct birds are shown in panels* ***A*** *(Black 111- blue trace),* ***C*** *(Cyan 12- Cyan trace),* ***E*** *(Red 240 – green trace),* ***G*** *(Yellow 15- yellow trace) and* ***I*** *(Red 240 – red trace) overlaid with the model simulations in each (black) after manual editing the results from the optimal values that is dependent on mean square error. The first spike morphologies for the same biological neurons shown in* ***A****,* ***C****,* ***E****,* ***G,*** *and* ***I*** *are shown in panels* ***B****,* ***D****,* ***F, H,*** *and* ***J*** *respectively overlaid with that of the corresponding model (black).*

The careful fitting procedure that had been conducted converged on an optimal set of parameters for the Na^+ and K^+ currents that best fit HVC_X neurons. Figure 11 shows the steady-state activation and inactivation functions for their fast gating variables (m_∞, h_∞, n_∞). This constitutes an improvement in the modeling paradigms of this class of HVC neurons which is important for our next steps and future modeling of this nucleus.

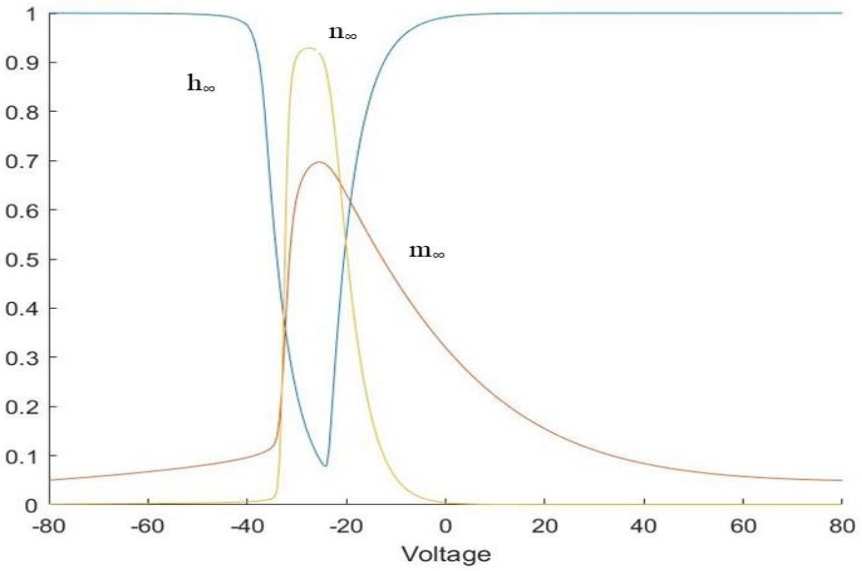

***Figure 11**: Steady-state activation functions for the fast gating variables that controls the activation/inactivation kinetics of the Na^+ and K^+ currents.*

Previous results have showed that in response to injections of the canonical depolarizing currents, the spike patterns for HVC_X neurons of a given bird all tended to have similar onsets, numbers of spikes, and timing of spikes, whereas these characteristics varied from bird to bird (Daou and Margoliash 2020). Examining the distribution of predicted current magnitudes (manual fitting) for the five ion channels revealed that the neurons from each animal occupied a small volume in the five-dimensional space of ion conductance magnitudes, and that there were large differences

between animals (Daou and Margoliash 2020). This is anticipated from the variation of spike waveforms and spike trains described above, but here is expressed in terms of magnitudes of plausible, pharmacologically confirmed HVC_X ion currents. While these results showed clear clustering for the maximal conductances for the ionic currents, it left the details of the kinetics of the ionic currents themselves not clear.

To this end, we checked the distribution of the magnitudes for the 7 key parameters that controls the Na^+ and K^+ currents activation/inactivation kinetics after the manual editing process. The scatter plots for the varied parameters are shown in Fig. 12 for all neurons from all birds. While the clustering for the maximal conductances is not surprising (Fig. 12A-B) and had been reported before (Daou and Margoliash 2020), it was surprising for us that even the parameters that control the activation kinetics of the Na^+ and K^+ currents showed tight clustering that were homogenous within the same bird and heterogeneous across birds (Fig. 12C-F).

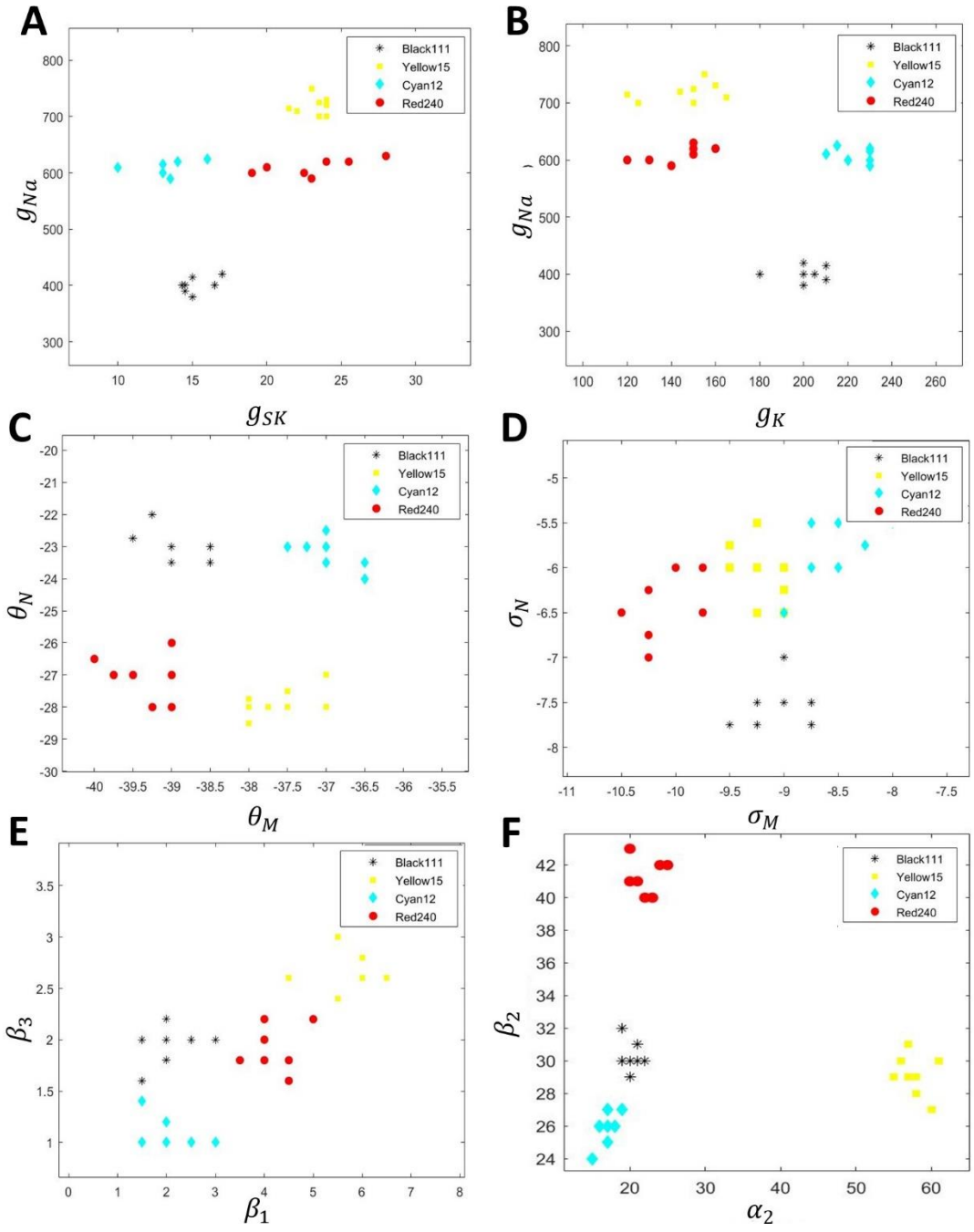

Figure 12**: Uniformity between modeled neurons from the same bird and different clustering across each other. A scatter plot of 30 manually modeled neurons showing the main parameters that varied the most across the population,* ***A *(g_{Na}vs g_{SK}),* ***B*** *(g_{Na}vs g_K),* ***C*** *($\theta_N$vs θ_M),* ***D*** *($\sigma_M$vs σ_N),* ***E*** *(β_1 vs β_3), and* ***F****(α_2 vs β_2). These different 4 animals (Black 111, Yellow 15, Cyan 12, and Red 240) are denoted by different symbols and colors (Black stars, Yellow squares, Cyan diamonds, and Red circles) where they occupy different regions in the 2D space.*

The homogeniety of the half-activation and half-inactivation kinetic parameters within the same bird and their heterogeniety across birds is an unpredecented result in the field. These parameters govern the the ranges of voltage domains where the Na^+ and the K^+ currents are activated. In particular, the half-activation/inactivation represents the time at which the half-maximal current amplitude is evoked and the sigma's represent how steep this activation/inactivation is, that is, how long does the activation/inactivation function remain open. Our accurate fitting of the voltage traces using these parameters showed us that not only the maximal conductances tightly cluster across the different HVC_X neurons within the same bird, but also every associated parameter that orchestrate these ionic currents. It shows us also that the internal house of the neuron, that is, its intrinsic properties, is a much more complex process that we originally thought of and opens new venues for research.

CHAPTER V

CONCLUSION

We have developed here a single compartment conductance-based model which replicated most of the neurophysiological firing patterns and properties of HVC neurons in the zebra finch that can be used in future studies to unveil the intricate circuitry that governs the overall process of bird's song. The modeled neurons are able to capture the spikes' timing as well as the details of the spikes' morphology and heuristics such as: spike amplitude, threshold, spike width, depolarization and repolarization segments. The careful fitting conducted unveiled important details about the intrinsic properties that these neurons exhibit in singing birds and built up on recent results that related ionic currents' magnitudes to features of song such as the homogeneity with in same individual and heterogeneity across other individuals. We showed that not only the maximal conductances tightly cluster across the different HVC_X neurons within the same bird, but also the half-activation and half-inactivation kinetic parameters that orchestrate these ionic currents.

However, this work highlighted many of the key challenges that any computational neuroscientist may face and raised up new questions that still need to be tackled to unravel more important information in this area. It is vital to know what is considered an "appropriate" level of abstraction to build models in neuroscience? Also, are we to build mathematical models with as many parameters as possible to take into account every single aspect of the biology? or are we to consider simplistic models that aim to extract the key principles of neuronal properties? Should we aim to predict the spike timing of every neuron with millisecond precision or rather to characterize more

global aspects of the network behavior? And what is considered a “best fit” for a model when attempting to replicate a biological pattern? Given the huge nonlinearities that are exhibited in biological models, these questions are touchstone. Detailed and accurate models are much needed to emulate the neuronal firing patterns observed *in vitro* not only for HVC_X neurons but also for many other classes of neurons. Therefore, generating a biophysically realistic model for this class of neurons will have a huge impact on the field as we’ll be able to integrate it in network studies to unveil larger questions on the nature of the intricate circuitry that governs the behavior of this nucleus and ultimately the bird’s song.

REFERENCES

Abarbanel, H. D., et al. (2004). "Spike timing and synaptic plasticity in the premotor pathway of birdsong." Biol Cybern 91(3): 159-167.

Abarbanel, H. D., et al. (2004). "Dynamical model of birdsong maintenance and control." Phys Rev E Stat Nonlin Soft Matter Phys 70(5 Pt 1): 051911.

Daou, A. and D. Margoliash (2020). "Intrinsic neuronal properties represent song and error in zebra finch vocal learning." Nat Commun 11(1): 952.

Daou, A., et al. (2013). "Electrophysiological characterization and computational models of HVC neurons in the zebra finch." J Neurophysiol 110(5): 1227-1245.

Destexhe, A. and A. Babloyantz (1993). "A model of the inward current Ih and its possible role in thalamocortical oscillations." Neuroreport 4(2): 223-226.

Donze, A., et al. (2010). "Parameter synthesis in nonlinear dynamical systems: application to systems biology." J Comput Biol 17(3): 325-336.

Drew, P. J. and L. F. Abbott (2003). "Model of song selectivity and sequence generation in area HVc of the songbird." J Neurophysiol 89(5): 2697-2706.

Dutar, P., et al. (1998). "Multiple cell types distinguished by physiological, pharmacological, and anatomic properties in nucleus HVc of the adult zebra finch." J Neurophysiol 80(4): 1828-1838.

Gibb, L., et al. (2009). "Brain stem feedback in a computational model of birdsong sequencing." J Neurophysiol 102(3): 1763-1778.

Gibb, L., et al. (2009). "Inhibition and recurrent excitation in a computational model of sparse bursting in song nucleus HVC." J Neurophysiol 102(3): 1748-1762.

Hodgkin, A. L. and A. F. Huxley (1952). "A quantitative description of membrane current and its application to conduction and excitation in nerve." J Physiol 117(4): 500-544.

Jin, D. Z. (2009). "Generating variable birdsong syllable sequences with branching chain networks in avian premotor nucleus HVC." Phys Rev E Stat Nonlin Soft Matter Phys 80(5 Pt 1): 051902.

Katahira, K., et al. (2007). "A neural network model for generating complex birdsong syntax." Biol Cybern 97(5-6): 441-448.

Katz, L. C. and M. E. Gurney (1981). "Auditory responses in the zebra finch's motor system for song." Brain Res 221(1): 192-197.

Kubota, M. and I. Taniguchi (1998). "Electrophysiological characteristics of classes of neuron in the HVc of the zebra finch." J Neurophysiol 80(2): 914-923.

Lewicki, M. S. (1996). "Intracellular characterization of song-specific neurons in the zebra finch auditory forebrain." J Neurosci 16(18): 5855-5863.

Lewicki, M. S. and M. Konishi (1995). "Mechanisms underlying the sensitivity of songbird forebrain neurons to temporal order." Proc Natl Acad Sci U S A 92(12): 5582-5586.

Li, M. and H. Greenside (2006). "Stable propagation of a burst through a one-dimensional homogeneous excitatory chain model of songbird nucleus HVC." Phys Rev E Stat Nonlin Soft Matter Phys 74(1 Pt 1): 011918.

Long, M. A., et al. (2010). "Support for a synaptic chain model of neuronal sequence generation." Nature 468(7322): 394-399.

Mansouri, M. M., et al. (2014). "Modeling of nonlinear biological phenomena modeled by S-systems." Math Biosci 249: 75-91.

Mattei, T. A. (2014). "Unveiling complexity: non-linear and fractal analysis in neuroscience and cognitive psychology." Front Comput Neurosci 8: 17.

Meunier, C. and I. Segev (2002). "Playing the devil's advocate: is the Hodgkin-Huxley model useful?" Trends Neurosci 25(11): 558-563.

Mooney, R. (2000). "Different subthreshold mechanisms underlie song selectivity in identified HVc neurons of the zebra finch." J Neurosci 20(14): 5420-5436.

Mooney, R., et al. (2001). "Auditory representation of the vocal repertoire in a songbird with multiple song types." Proc Natl Acad Sci U S A 98(22): 12778-12783.

Mooney, R. and J. F. Prather (2005). "The HVC microcircuit: the synaptic basis for interactions between song motor and vocal plasticity pathways." J Neurosci 25(8): 1952-1964.

Schmidt, M. F. and D. J. Perkel (1998). "Slow synaptic inhibition in nucleus HVc of the adult zebra finch." J Neurosci 18(3): 895-904.

Shea, S. D., et al. (2010). "Neuron-specific cholinergic modulation of a forebrain song control nucleus." J Neurophysiol 103(2): 733-745.

Solis, M. M. and D. J. Perkel (2005). "Rhythmic activity in a forebrain vocal control nucleus in vitro." J Neurosci 25(11): 2811-2822.

Terman, D., et al. (2002). "Activity patterns in a model for the subthalamopallidal network of the basal ganglia." J Neurosci 22(7): 2963-2976.

Troyer, T. W. and A. J. Doupe (2000). "An associational model of birdsong sensorimotor learning II. Temporal hierarchies and the learning of song sequence." J Neurophysiol 84(3): 1224-1239.

Wang, H., et al. (2013). "Equilibrium analysis and phase synchronization of two coupled HR neurons with gap junction." Cogn Neurodyn 7(2): 121-131.

Wang, X. J., et al. (2003). "Adaptation and temporal decorrelation by single neurons in the primary visual cortex." J Neurophysiol 89(6): 3279-3293.

Wild, J. M., et al. (2005). "Calcium-binding proteins define interneurons in HVC of the zebra finch (Taeniopygia guttata)." J Comp Neurol 483(1): 76-90.

Yi, G. S., et al. (2014). "Neuronal spike initiation modulated by extracellular electric fields." PLoS One 9(5): e97481.